Electronic and spectroscopic properties of the hydrogen-terminated Si(111) surface from *ab initio* calculations

Yan Li[1,*] and Giulia Galli[1,2]

[1]*Department of Chemistry, University of California, Davis, Davis, California 95616, USA*

[2]*Department of Physics, University of California, Davis, Davis, California 95616, USA*

(Received 12 May 2010; revised manuscript received 26 June 2010; published 30 July 2010)

We report on a detailed, theoretical study of the electronic and spectroscopic properties of the hydrogen-terminated Si(111) surface. We computed band structures and scanning tunneling microscopy (STM) images, and we analyzed the performance of density-functional theory within the local-density approximation (LDA), and of many-body perturbation theory (at the GW level) in interpreting and rationalizing experimental results. We discuss numerical approximations involved in the implementation of the two theoretical approaches, and the need to control them with extreme care, to reach a robust assessment of the theory. We find that although at the LDA level severe discrepancies with experiment are present, in the description of the surface electronic states, the STM images computed using GW and LDA band structures are qualitatively the same. Computed constant height STM images in close proximity of the surface exhibit bright, round spots on top of H atoms while low-temperature measurements show triangular spots. Our results suggest that to reproduce these triangular shapes, one may need to explicitly consider tip-surface interactions and that the tip-sample distance may as well play a role in determining experimental images. Computed current-voltage characteristics are in qualitative agreement with experiment.

DOI: 10.1103/PhysRevB.82.045321 PACS number(s): 73.20.At, 71.10.−w, 71.20.−b, 74.55.+v

I. INTRODUCTION

Modification and/or functionalization of silicon surfaces provide a useful means to control the performance of several silicon-based devices, for example, Si rods used as photo-electrodes in photoelectrochemical and photovoltaic applications.[1,2] Most of the current experimental efforts are concentrated on relatively complex functionalizations, e.g., methylation of Si(111) surfaces, providing protection from oxidation,[3,4] and mixed methyl/allyl monolayers on Si(111), allowing for secondary reactivity through the unsaturated allyl groups.[5] Several *ab initio* calculations of functionalized Si surfaces have also appeared in the recent literature.[6–8] However, a thorough, theoretical understanding of the electronic properties of the simplest silicon surfaces, i.e., those saturated by hydrogen atoms, has not yet been achieved, although several papers have provided valuable information on surface states.[9,10] For example, a one-to-one comparison with experiment in the case of measured scanning tunneling microscopy (STM) images and scanning tunneling spectroscopy (STS) characteristics of the hydrogen-terminated Si(111) surface [H-Si(111)] has not yet been carried out. Such comparisons with experiment are very important prerequisites to assess the validity and predictive capabilities of first-principles theories used for the description of more complex, functionalized silicon surfaces.

In this paper, we report on a detailed, theoretical study of the electronic and spectroscopic properties of the H-Si(111). This is a substrate that is usually obtained experimentally[4] by etching oxidized silicon in HF under high pH conditions, and perfectly saturated, unreconstructed surfaces may be obtained. We computed band structures, STM images, and STS characteristics and we first analyzed the performance of different levels of theory to rationalize experimental results. In particular, we compared calculations carried within density-functional theory (DFT), in the local-density approximation (LDA), and calculations using many-body perturbation theory at various GW levels. We investigated the numerical approximations involved in the implementation of the two theoretical approaches, whose detailed control turns out to be critical for a robust assessment of the theory in the description of electronic properties of the H-Si(111) surface. As expected, our results at the LDA level show severe discrepancies with experiment in describing several electronic states of this surface. However, the STM images computed using GW and LDA band structures are qualitatively the same. When computing constant height STM profiles in close proximity of the surface, we find bright round shapes in correspondence of H atoms, in agreement with experiments carried out at room temperature,[11] but at variance with recent low temperature, low current STM measurements which show triangular spots.[12] Based on the analysis of the tunneling current dependence on tip geometry and its distance from the surface, we suggest that in order to explain the difference between measured and computed STM patterns,[11,12] one needs to explicitly consider tip-surface interactions and the tip-sample distance. We also computed STS characteristics, which are in qualitative agreement with experiment.

The rest of the paper is organized as follows. We first describe the method and geometrical models used in our calculations (Sec II). Then we present our results for electronic and spectroscopic properties of the H-Si(111) surface in Secs. III and IV, respectively. Finally, a summary of our findings in Sec. V concludes the paper.

II. METHOD

We carried out DFT calculations with the QUANTUM ESPRESSO package,[13] using norm-conserving pseudopotentials, local-density (LDA) exchange and correlation function-

 ©2010 The American Physical Society

als, and plane-wave basis sets with a kinetic-energy cutoff of 16 Ry. A $8\times8\times1$ and a $24\times24\times1$ Monkorst-Pack[14] k-point grids were used to sample the Brillouin zone for ground-state calculations, and for computing band structures and density of states, respectively. Fully covered, hydrogen-terminated Si(111) surfaces were modeled by symmetric slabs, at the experimental bulk lattice constant (5.43 Å). A vacuum region equivalent to four atomic layers was used to avoid spurious interactions between replicas. The H layers and the first three Si layers on each side of the slab were fully relaxed till the minimum force was smaller than 0.026 eV/Å.

The calculation of the tunneling current I at an applied sample bias V was approximated by a simple integral of the surface local density of states (LDOS) at the tip position,[15]

$$I \propto \int_{E_F}^{E_F+eV} dE \rho_s(r,E), \qquad (1)$$

where $\rho_s(r,E)=\Sigma_i|\Psi_i(r)|^2\delta(E_i-E)$ is the unperturbed (zero applied bias) surface LDOS at energy E and tip position r, and $\Psi_i(r)$ and E_i are the one-electron wave function and eigenvalue. The Fermi level E_F is defined as the energy position in the middle of the band gap.

Many-body perturbation-theory calculations at the GW level were performed using the ABINIT code;[16,17] we used a 12-layer, relaxed H-terminated Si(111) slab. A k grid of $6\times6\times1$ and a kinetic-energy cutoff of 16 Ry were used for LDA ground-state calculations. LDA energy eigenvalues and wave functions were then used to construct the inverse dielectric matrix $\epsilon^{-1}_{G;G'}$ (G and G' indicate reciprocal-lattice vectors) and perturbatively evaluate the self-energy operator Σ at the G_0W_0 level. An energy cutoff of 10 Ry was used to expand the wave functions in the evaluation of ϵ and Σ, and 670 empty bands were included. The same energy cutoff was used to represent ϵ and Σ, yielding matrices of size of 1287×1287. The matrix ϵ was generated on a $6\times6\times1$ q grid, which corresponds to seven special points in the irreducible Brillouin edge including $\bar{\Gamma}$, $\bar{K}$, and $\bar{M}$. We have checked that further increasing the cutoff energy to 16 Ry or the q-point grid to $8\times8\times1$ has a negligible influence on the values of computed GW self-energy corrections (differences are within 0.05 eV). Convergence of computed quasiparticle energies as a function of the number of empty electronic states used to compute the ϵ and Σ matrices, was tested by comparing values obtained with 350 and 670 empty states; for all cases considered here the differences were at most 0.05 eV. We also performed partially self-consistent calculations within the GW_0 approximation, where the eigenenergies in the Green's function were updated self-consistently. We chose this level of self-consistency based on results obtained for bulk Si (see the Appendix). The frequency integration was performed by the contour deformation method,[18] with 20 and 4 frequencies along the real and imaginary axes, respectively. Comparisons were made to results obtained using various plasmon-pole models (PPMs) such as those proposed by Godby and Needs (GN) (Ref. 19) or Hybertsen and Louie (HL) (Ref. 20) and they will be discussed below. Similar studies were performed for bulk Si (see the Appendix).

TABLE I. Computed band gaps (in eV) of the H-Si(111) surface at the LDA and G_0W_0 level, using slabs of different thicknesses, compared with that of bulk silicon. The number of Si layers in the slab is denoted by nL.

nL	6	12	18	30	Bulk
E_g^{LDA}	1.0	0.73	0.66	0.62	0.52
$E_g^{G_0W_0}$	1.9	1.5	1.4		1.2

The self-energy correction for orbital i was computed as $\delta E_i=\langle\Psi_i|\Sigma(E_i)-V_{xc}|\Psi_i\rangle$, where V_{xc} is the LDA exchange-correlation potential and $|\Psi_i\rangle$ is the LDA wave function of orbital i. Depending on the level of self-consistency on the eigenenergies, E_i in $\Sigma(E_i)$ refers to either the Kohn-Sham eigenenergy E_i^{KS} or the updated quasiparticle eigenenergy E_i^{QP}.

III. ELECTRONIC STRUCTURE OF H-Si(111)

At the LDA level, we find a H-Si bond length of 1.53 Å for H-Si(111) slabs containing 6–30 Si layers, in agreement with previous calculations.[10] While the thickness of the slab has little influence on the structural properties of the surface, the electronic properties are much more sensitive to the choice of the slab model. In Table I, we report the calculated LDA band gap using different numbers of Si layers in the slab model (that we denote by nL). The band gap shows an almost inverse-linear variation with the slab size, similar to that observed in LDA calculations of hydrogen-terminated Si(100) slabs.[21] The band gap of bulk silicon was calculated to be 0.52 eV, consistent with the previously reported value of 0.51 eV.[22] As well known, the calculated LDA band gap is significantly underestimated with respect to the experimental value ($E_g^{exp}=1.17$ eV) while at the G_0W_0 level, one finds good agreement with experiment ($E_g^{G_0W_0}[\text{bulk}]=1.2$ eV) (see also Table III). In order to obtain results converged as a function of slab size, we adopted a 30-layer slab for the LDA calculations of the band-structure and spectroscopic properties discussed below, unless specified otherwise. For perturbative or partially self-consistent GW band-structure calculations, we instead chose a 12-layer slab to reduce the computational cost; using this number of layers yields a reasonably converged electronic structure of *occupied* states and does not qualitatively change the conclusions on the spectroscopic features of the surface with respect to using a larger number of layers. For example, differences in G_0W_0 self-energy corrections obtained with $nL=12$ and $nL=18$ are within 0.05 eV.

The computed LDA band structure of H-Si(111) is shown in Fig. 1 along the high-symmetry line $\bar{\Gamma}$-$\bar{K}$-$\bar{M}$. We found bands of surface states between $\bar{K}$-$\bar{M}$ at about 3, 4, and 8 eV below the valence-band maximum (VBM), as indicated by the arrows. Corresponding peaks are visible in the projected density of states (PDOS) of the hydrogen atoms and the first-layer Si atoms. Similar energy positions of surface states were obtained for the methyl-terminated Si(111) surface [CH_3-Si(111)] from DFT/generalized gradient approxima-

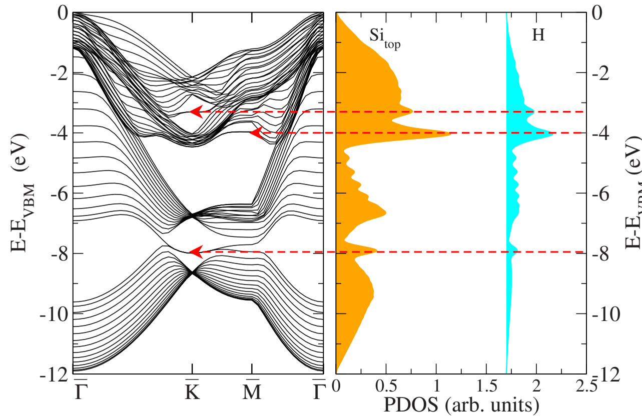

FIG. 1. (Color online) Band structure computed within LDA (left) and PDOS (right) of the H-Si(111) surface. Energy positions of representative surface states at high-symmetry points $\bar{K}$ and $\bar{M}$ are indicated by red arrows. PDOS of first-layer Si atoms and that of H atoms are both shown.

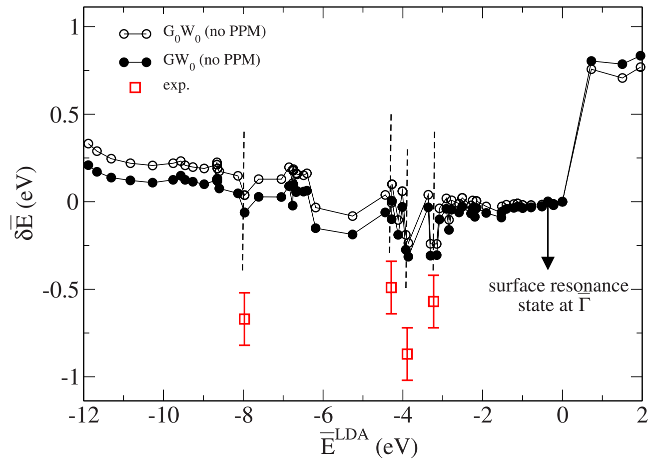

FIG. 2. (Color online) Computed self-energy corrections (δE) at the $G_0(G)W_0$ level, as a function of LDA orbital energies (E^{LDA}). The dashed, vertical lines indicate the positions of surface states at $\bar{K}$ and $\bar{M}$. Corrections needed to match measured surface energy levels (Ref. 23) are shown by red squares, with error bars taken as the approximate half width (~0.15 eV) of the peak observed in photoemission spectra. The position of the surface resonance state at $\bar{\Gamma}$ is indicated by a black arrow.

tion calculations.[15] As wave functions of such surface states are mainly localized on the first two Si layers, and exhibit small or moderate hybridization with the adsorbate, the property and energy positions of these states are not sensitive to the type of adsorbate, e.g., whether atomic hydrogen or a methyl group. However, in the case of the CH_3-Si(111) surface, additional surface states were found which correspond to molecular orbitals that are only weakly hybridized with the silicon substrate.[15]

Photoemission experiments[23] and previous many-body perturbation-theory calculations within the GW approximation[10] yield surface states that are lower in energy by 0.5–0.9 eV, with respect to those predicted by LDA calculations. Our G_0W_0 and GW_0 calculations for the energy position of surface states, shown in Table II and Fig. 2, yield results similar to experiments and previous studies, although the magnitude of self-energy corrections found in our work differ by 0.3–0.5 eV from those of Ref. 10. We ascribe this difference to the use of the generalized plasmon-pole model approximation of Hybertsen and Louie[20] in Ref. 10, which lowers the energy positions of surface states by 0.1–0.4 eV, compared with results obtained by direct frequency integration techniques (see Table II). The discrepancy between our results and those of Ref. 10 is more evident at the GW_0 level and for surface states deeper in energy; this finding is consistent with the large difference of valence-band width found in calculations using PPMs and direct integration, for both H-Si(111) and bulk Si (see Table III). The explicit frequency dependence employed in the direct integration, although more accurate than the use of PPMs, yields valence-band width and surface states (in particular, low-lying ones) in apparently worse agreement with experiments. The relatively poor agreement with experiment may be partly caused by use of pseudopotentials as well as by the $G_0W_0(GW_0)$ approxi-

TABLE II. Quasiparticle energies computed at the $G_0W_0(GW_0)$ level for a 12-layer H-Si(111) slab. We report the valence-band width (E_W), the band gap between $\bar{\Gamma}$ and $\bar{M}$($E_g^{\bar{\Gamma}\text{-}\bar{M}}$), and energies of surface states at $\bar{K}$ and $\bar{M}$ relative to the VBM (see Fig. 1). Frequency integrations were performed with the contour deformation method (Ref. 18) (no PPM) or by the use of plasmon-pole models proposed by Godby and Needs (Ref. 19) (GN) and by Hybertsen and Louie (Ref. 20) (HL). All energies are in electron volt.

	$G_0W_0(GW_0)$					
	No PPM	GN	HL	HL[a]	HL (Ref. 10)	Expt. (Refs. 23 and 24)
E_W	11.6 (11.7)	11.3 (11.3)	11.8 (12.0)	11.9 (12.1)		12.5±0.6
$E_g^{\bar{\Gamma}\text{-}\bar{M}}$	1.46 (1.53)	1.45 (1.54)	1.48 (1.57)	1.32 (1.41)		1.32
$\bar{K}$	−3.49 (−3.54)	−3.52 (−3.57)	−3.62 (−3.69)	−3.68 (−3.75)	−3.82	−3.80
	−4.37 (−4.44)	−4.43 (−4.49)	−4.49 (−4.57)	−4.62 (−4.68)	−4.76	−4.78
	−7.96 (−8.03)	−8.04 (−8.10)	−8.28 (−8.44)	−8.38 (−8.52)	−8.47	−8.64
$\bar{M}$	−4.13 (−4.19)	−4.18 (−4.24)	−4.30 (−4.38)	−4.38 (−4.46)	−4.63	−4.76

[a]Parameters used for GW calculations were extracted from Ref. 10, with 350 empty states and energy cutoffs of 11.6 Ry, 7.8 Ry and 4.4 Ry for ϵ, bare exchange, and dynamical part of Σ, respectively.

mations, as discussed in the Appendix. Other factors, e.g., the energy cutoff and the number of conduction bands used to evaluate the dielectric matrix and self-energy operator, may also result in additional differences of 0.1–0.2 eV between our results and those present in the literature. Overall, our best-converged $G_0W_0(GW_0)$ results are within error bars determined by experimental uncertainty, and numerical uncertainties involved in the evaluation of self-energy corrections at the $G_0W_0(GW_0)$ level.

IV. SPECTROSCOPIC PROPERTIES OF H-Si(111)

Computed STM images using LDA eigenvalues and wave functions are shown in Fig. 3. Experiments were conducted at a bias of −2.5 V.[12] Our calculations were carried out with a bias of −1.0 V. We note that, in principle, one cannot expect a one-to-one correspondence between the applied sample bias in experiments and that in our simulations, because of the underestimate of the band gap within LDA, and of tip-induced band bending (TIBB) effects present in experiments.[25] In addition, the exact position of the Fermi level in the experimental samples is not known. Assuming $|E_F - E_v| = 1.04$ eV as determined for similarly doped bulk Si samples[26] and negligible TIBB effects at negative bias (due to narrow accumulation layers for n-doped Si), a sample bias of −2.5 V in the experiments corresponds to an energy about 1.5 eV below the VBM. Since $|E_F^{\text{theo}} - E_v| = 0.3$ eV according to our definition of the theoretical position of the Fermi level $E_F^{\text{theo}} \equiv (E_{\text{VBM}} + E_{\text{CBM}})/2$, we applied a sample bias of −1.0 V to mimic the experimental bias of −2.5 V. Under such bias [Fig. 3(a)], we obtain triangular shapes similar to experiment in computed STM images at a distance of 1 Å from the surface, if we use only six layers to represent our slab. This apparent good agreement is accidental. At low negative bias ($-3 < V_{\text{bias}} < 0$ V), the main contribution to the tunneling current comes from bulklike surface resonance states near the $\bar{\Gamma}$ point (see Fig. 2). Such states, although coupled to the adsorbate orbitals, are distinguished from true surface states as they are delocalized across the entire slab in the same way pure bulk states are. For $nL = 6$, energy positions of the electronic states are strongly influenced by finite-size effects. As a result, the surface PDOS does not have any contributions from surface resonance states in the vicinity of the Fermi level (Fig. 4). Therefore, the simulated STM image at $nL = 6$ mostly contains signals arising from PDOS contributions from the Si substrate, exhibiting threefold symmetry and thus producing triangular-shaped features. As nL increases, the contribution of H atoms to the PDOS increases near the Fermi level, and at $nL = 30$, the simulated STM image at a constant height of 1 Å shows round spots [Fig. 3(b)], corresponding to PDOS contributions from H atoms. This is in agreement with room-temperature STM measurements[11] but at variance with experimental images obtained at 77 K showing triangular spots.[12]

Therefore, we analyzed whether the triangular-shaped features observed in the experiment[12] may arise from tip-surface interactions present in the measurements but not included in the calculations; we also investigated effect of the tip-sample distance in the measurements. We first replaced the LDOS at

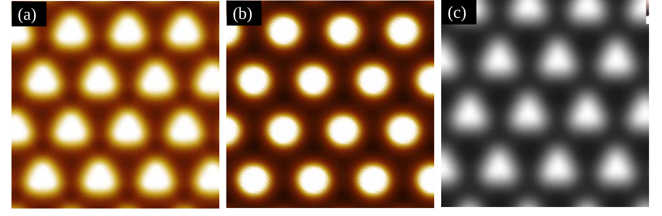

FIG. 3. (Color online) Constant height (1 Å) STM images of the H-Si(111) surface computed with slabs containing 6 [(a)] and 30 [(b) and (c)] layers. In (c), the tunneling current was averaged over the vertices of an equilateral triangle of side length $a = 2.77$ Å to mimic a triangular Pt tip. Sample bias is −1.0 V.

location r in the expression for the tunneling current $I(r)$ [Eq. (1)] by an average value over a finite grid representing symmetry and spatial extent of a model tip.[27] The resulting STM images dramatically change. For example, by averaging the tunneling current over the vertices of an equilateral triangle of side length $a = 2.77$ Å, representing the interatomic distance in triangular Pt/Ir STM tips used in the experiment,[12] we find an STM image clearly showing the triangular symmetry of the tip geometry. The center of the bright triangular spots in Fig. 3(c) is not located on top of the hydrogen atoms but is instead shifted in correspondence of the fcc site. A similar influence of the tip electronic structure was found in the case of Ag on Si(111), where STM patters were found to be strongly influenced by tips represented by tungsten clusters with different apex geometry.[28] Another possible reason for the observed triangular features may be related to the spatial extent of the tip (Pt or Ir) orbitals and their overlap with those of the dense adsorbate. For example, earlier calculations have shown that sulfur atoms on Re(0001) may be imaged either as bright spheres or triangles, depending on whether the tip apex is modeled with a single S atom or a single Pt atom, in agreement with measured STM patterns under similar scanning condition.[29] STM patterns may also

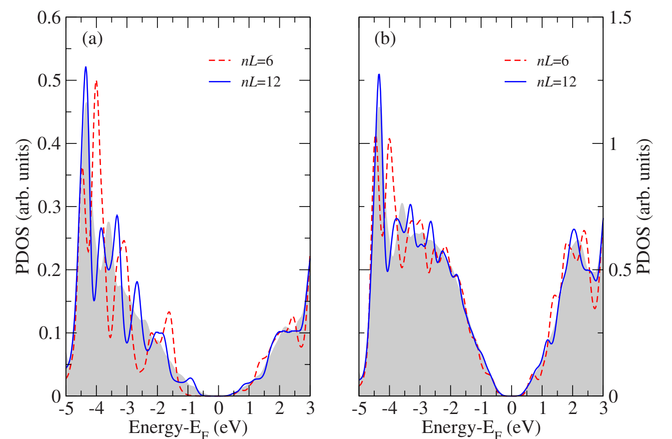

FIG. 4. (Color online) PDOS of the H-Si(111) surface computed within LDA at various slab thickness: $nL = 6$ (red dashed curve), 12 (blue curve), and 30 (shaded curve). PDOS from H atoms (a) clearly shows a strong finite-size effect close to the Fermi level E_F at small nL. In contrast, PDOS from the first-layer Si atoms (b) is already well converged at $nL = 12$ in the vicinity of E_F. Here E_F is defined as the energy position in the middle of the band gap.

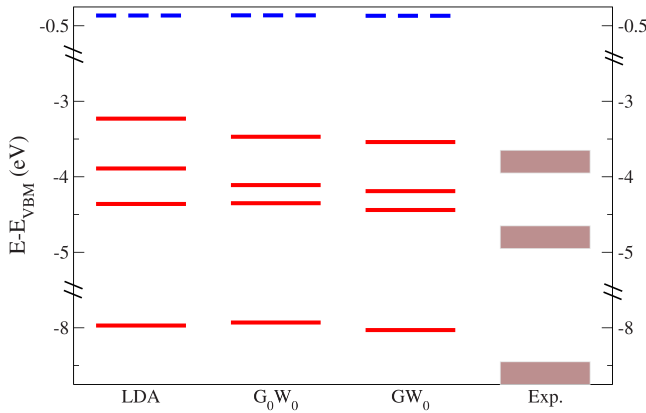

FIG. 5. (Color online) Energy levels of surface states at $\bar{K}$ and $\bar{M}$ (red solid line) (see Fig. 1) and the surface resonance state at $\bar{\Gamma}$ (blue dashed line) relative to the valence-band maximum, as predicted by three different levels of theory: LDA, G_0W_0, and GW_0. Energy positions of measured surface states (Ref. 23) are shown as thick horizontal bars with thickness equal to the width (~0.3 eV) of experimental photoemission spectra.

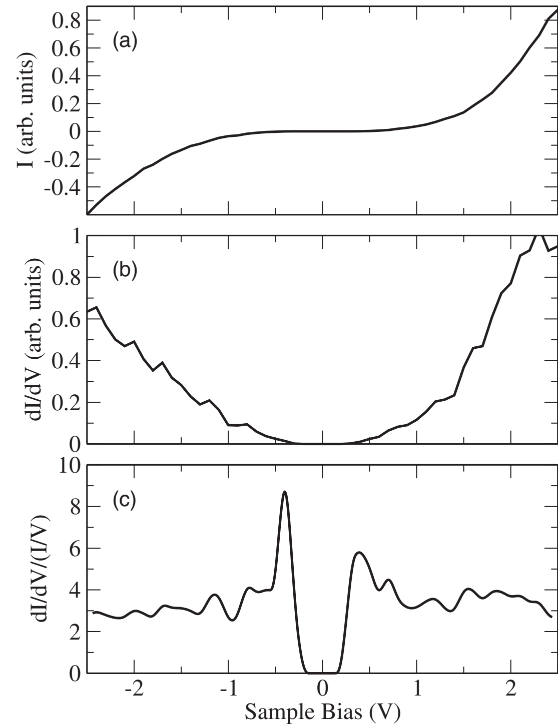

FIG. 6. Simulated current-voltage (*I-V*) characteristics for the H-Si(111) surface. Contributions from surface resonance states dominate the tunneling current, as shown by the wide gap and slowly decaying signal tails in (a) and (b). Contributions from the silicon substrate are enhanced in the normalized conductance $[dI/dV/(I/V)]$ shown in (c), revealing the fundamental gap of bulk silicon.

depend on tip-sample distance, which was not explored in the experiments.[12] Due to high packing density of the hydrogen atoms and interference effects, the tunneling current at fcc or hcp site may have significant contributions from neighboring hydrogen atoms. At large tip-sample distance, interference effects may give rise to spots with nonspherical shapes, and in our calculations we did observe triangularlike spots in STM images obtained at distances, e.g., of 5 Å from the surface. Finally, the influence of the tip-induced electric field, which was not explicitly accounted for in our calculations, may cause changes in STM contrast, as pointed out in the case of chemisorbed ethylene on the Si(001) surface.[30,31] However, since the tip apex and tip-sample distance used experimentally are not known, at present it is not possible to establish conclusively all of the reasons for the observed triangular-shaped features.

In order to investigate whether the computed STM images may be affected by a possibly inaccurate, relative position of surface and bulk states obtained within DFT/LDA, we further examined the G_0W_0 and GW_0 quasiparticle energies obtained for H-Si(111). For the 12-layer slab, the self-energy corrected band gap of the surface is increased by 0.7 eV with respect to the one computed at the LDA level (see Table I). Self-energy corrections to surface states are larger in magnitude by 0.2–0.3 eV than those to bulk states in the same energy range; thus surface states are shifted downward in energy, relative to the VBM, with respect to their corresponding positions found at the LDA level, as shown in Figs. 2 and 5. This is in agreement with previous results based on perturbative GW calculations.[10] On the other hand, the energy position of surface resonance states relative to VBM as obtained within LDA is almost unaffected by self-energy corrections because of their bulklike nature, with a change of a few millielectron volt. Therefore, the H-Si(111) STM images computed at the LDA level are very similar (and qualitatively the same) as those obtained within G_0W_0. Such insensitivity might be enhanced by the use of the Tersoff-Hamann approximation in Eq. (1), which provides a more approximate treatment of the electronic coupling between the tip and sample than more sophisticated tunneling formulas, e.g., based on Green's function techniques.

Finally, we present calculated current-voltage (*I-V*) characteristics of the H-Si(111) surface, as obtained with calculations with $nL=30$ (Fig. 6). As the tunneling conductance directly probes the LDOS at the tip position, its main contribution comes from the charge distribution on the adsorbate, due to the proximity of the tip and sample, similar to that observed in the simulated STM images. Indeed, the dI/dV plot displays a wide conductance gap with smoothly decaying edges, corresponding to the DOS contribution from hydrogen atoms. In contrast, the effect of tip-sample distance is partially canceled in the normalized conductance, and contributions from the silicon substrate become dominant close to the Fermi level, as clearly shown in Fig. 6(c). A much narrower and sharp gap is now present, and its magnitude is consistent with the calculated DFT band gap of the H-Si(111) surface with $nL=30$. The small peaks in the dI/dV and $dI/dV/(I/V)$ curves arise from those in the PDOS of H atoms and first-layer Si atoms. Similar to the case of STM images, in our GW calculations for the 12-layer H-Si(111) slab we find that self-energy corrections do not change the qualitative features of the *I-V* characteristics obtained from LDA. Within ±2.5 eV from $E_F \equiv (E_{VBM}+E_{CBM})/2$, the magnitude of self-energy corrections for valence (conduc-

tion) bands were found to differ from that of $E_{\mathrm{VBM}}(E_{\mathrm{CBM}})$ by less than 0.1 eV. Assuming similar differences in the case of the 30-layer H-Si(111) slab, we conclude that the *I-V* characteristics in Fig. 6 do not show any qualitative change at the GW level, except for the increase in the tunneling gap by about 0.7 eV (estimated from Table I). We note that our GW-corrected tunneling gap is still much smaller than the apparent gap found in STS measurements (2 eV) (Ref. 12) because of TIBB effects present in the experiments. It is not straightforward to include such effects in our calculations as band bending is usually not symmetric with respect to the polarity of the sample bias, especially when the sample is doped, as in the experiments of Yu *et al.*[12] However, the qualitative characteristics of the calculated current-voltage features, such as the absence of midgap states, are fully consistent with experiments.[12]

V. CONCLUSION

We have presented electronic-structure calculations of the H-terminated Si(111)-(1×1) surface, carried out by combining DFT and many-body perturbation theory within the G_0W_0 and GW_0 approximations. In particular, we examined the influence on the computed electronic and spectroscopic properties, such as simulated STM images and STS, of two main factors: finite-size effects of the slab model and the quasiparticle self-energy corrections. We found that the main contribution to the tunneling current comes from surface resonance states close to the Fermi level, which are weakly affected by self-energy corrections within many-body perturbation theory. Therefore, we obtain STM images and STS characteristics that are very similar and qualitatively the same at the LDA and G_0W_0 levels of theory. Theoretical images in close proximity of the surface exhibit bright, round spots on top of H atoms, in agreement with room-temperature measurements[11] but at variance with the triangular-shaped features observed in experiments carried out at 77 K with low tunneling current. We suggest that variations in STM patterns may be caused by the geometry and electronic structure of the tip, as well as by the tip-sample distance. It would be interesting to explore such effects with low temperature, high-resolution STM experiments.

ACKNOWLEDGMENTS

This work was funded by NSF under Grant No. CHE-0802907. Some of our calculations were performed at the NERSC and TeraGrid facilities. We thank A. Aliano, C. Fleming, H. Yu, and N. S. Lewis for useful discussions.

APPENDIX: QUASIPARTICLE SELF-ENERGY CORRECTIONS FOR BULK Si

In order to test the influence, on computed self-energy corrections (δE), of input single-particle orbitals and wave functions and of frequency integration techniques, we carried out GW calculations for bulk Si. In addition to energy levels in the vicinity of the VBM, we also examine δE of states close to the valence-band bottom, where the use of PPMs may not be a sensible approximation. A k grid of $4\times4\times4$ (corresponding to 19 special k points in the Brillouin zone) and a kinetic-energy cutoff of 24 Ry were used. Other parameters, such as the number of bands (n_{band}) and plane waves (n_{PW}) used to evaluate the screened Coulomb interaction W and the self-energy operator Σ were taken from Ref. 22, with $n_{\mathrm{band}}=35(100)$ for $W(\Sigma)$ and $n_{\mathrm{PW}}=169$. The frequency integration was performed by the contour deformation method[18] unless specified otherwise.

Table III lists computed DFT/LDA and GW energies of bulk silicon at high-symmetry points (in reduced coordinates): $\Gamma=(0,0,0)$, $X=(0,1/2,1/2)$, and $L=(1/2,0,0)$. Overall, our results are consistent with those in the literature.[22,33,34] We note that at the G_0W_0 level, the use of PPMs has little influence on the energy gaps in the vicinity

TABLE III. Energy levels of bulk silicon at high-symmetry points computed at the LDA and GW level. "G" (Green's function) and "W" (screened Coulomb interaction) without (or with) the subscript "0" correspond to quantities evaluated using self-consistently updated quasiparticle eigenvalues (or LDA eigenvalues). Wave functions were computed at the LDA level and were not updated except at the self-consistent QPscGW level. Energies (eV) are measured relative to the VBM. δE_{VBM} is the calculated *absolute* GW self-energy correction to the VBM energy level in LDA. Values in parentheses are pseudopotential calculations from Ref. 22; values in square brackets are full-potential linear muffin-tin orbital method from Ref. 32. See Table II for explanation of acronyms.

	LDA	$G_0W_0^{\mathrm{GN}}$	$G_0W_0^{\mathrm{HL}}$	G_0W_0	GW_0	GW	QPscGW	Expt. (Ref. 24)
$\lvert\Gamma_{1v}\rvert$	12.0	11.3	11.8	11.7 (11.4) [11.9]	11.7	11.9	11.9 (11.9) [12.2]	12.5 ± 0.6
Γ_{15c}	2.52	3.16	3.21	3.17 (3.20) [3.13]	3.25	3.41	3.49 (3.54) [3.45]	3.05,[b] 3.40
X_{1c}	0.61	1.25	1.29	1.27 (1.29) [1.11]	1.41	1.48	1.56 (1.60) [1.37]	1.326
L_{1c}	1.40	2.00	2.04	2.02 (2.08) [2.05]	2.16	2.24	2.32 (2.41) [2.32]	2.04
E_g	0.52	1.14	1.18	1.16 (1.14) [0.97]	1.23	1.39	1.45 (1.47) [1.23]	1.17
E_g(PAW)[a]				1.12	1.20	1.28	1.41	
δE_{VBM}		−0.35	−0.62	−0.37		−0.42	−0.49	−0.50

[a]References 33 and 34.
[b]Reference 35.

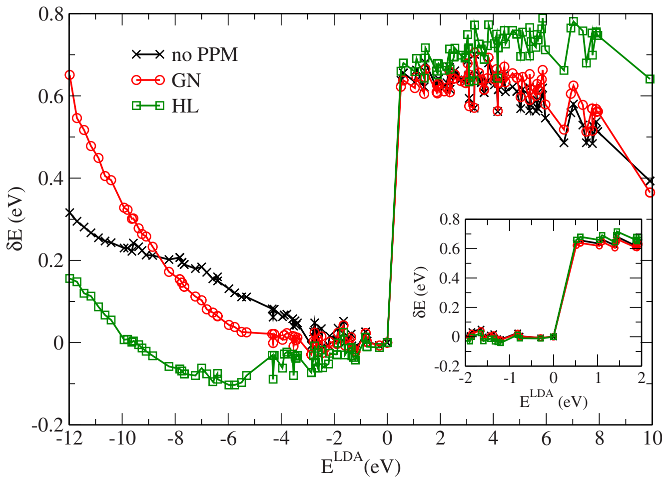

FIG. 7. (Color online) Self-energy corrections (δE) computed at the G_0W_0 level as a function of LDA orbital energies (E^{LDA}). Energies are relative to the valence-band maximum. See Table II for explanation of acronyms.

of VBM, with differences within 0.05 eV compared to those obtained by integration with contour deformation method (see inset of Fig. 7). However, the choice of PPMs has a much larger impact on the *absolute* value of the self-energy corrections. For example, δE_{VBM} calculated using the PPM proposed by Godby and Needs[19] is very close to that obtained with the contour deformation method ($\delta E_{\mathrm{VBM}} \approx -0.4$ eV) while δE_{VBM} calculated with the PPM proposed by Hybertsen and Louie[20] is much larger ($\delta E_{\mathrm{VBM}} \approx -0.6$ eV). Such differences in self-energy corrections between the different PPMs may affect properties which involve energy-level alignments between different materials, e.g., band offsets at heterosurfaces[36] or quasiparticle excitation energies (ionization potential or electron affinity).[37]

As one moves away from the vicinity of VBM, self-energy corrections, δE, predicted by different PPMs differ significantly, as shown in Fig. 7 where they are reported as a function of LDA eigenvalues, E^{LDA}. The difference in the values obtained for δE arising from the use of PPMs can be as large as 0.3–0.4 eV; for example, the valence-band width is predicted to be 11.7 (no PPM), 11.3 (GN), and 11.8 (HL) eV. Such large differences are not surprising as the use of PPMs is expected to be valid only for energies close to the energy gap. Therefore, care should be exercised when comparing with experiments GW-corrected energy levels obtained using PPMs, especially at energies far from the VBM. In some cases, the good performance of certain PPM may stem from cancellation of errors coming from other approximations involved in the calculation, e.g., lack of self-consistency and/or vertex corrections, and the use of pseudopotentials.

Next we examine the influence of the self-consistent treatments of eigenenergies and wave functions on δE. As shown in Table III, as one increases the level of self-consistency ($G_0W_0 \rightarrow GW_0 \rightarrow GW \rightarrow$ QPscGW), the energy gaps become larger while δE_{VBM} becomes more negative. QPscGW corresponds to self-consistent static approximation to the GW self-energy.[32] The computed valence-band width also shows a systematic increase, approaching experimental values. On the other hand, better self-consistency in GW calculations does not necessarily yield results in better agreement with experiments, as it still lacks the description of electron-hole interactions, in contrast to the GWΓ approximation which includes electron-hole interactions through vertex corrections. It was proposed[34] that the partially self-consistent GW_0 approximation is a relatively cheaper and reasonably accurate alternative to fully self-consistent GWΓ approximation for the prediction of band gaps for bulk Si and other semiconductor/insulators because of error cancellations from lack of electron-hole interaction and of self-consistent treatment of the screened Coulomb interaction W. Indeed, from Table III, one observes that most experimental values, including the band gap, fall in between those obtained from G_0W_0 and GW_0 calculations, except for the valence-band width. It may be interesting to explore how the calculated value of the latter may be affected by self-consistency and dynamical vertex corrections.[38]

Finally, we discuss the influence of treating core electrons in the pseudopotential scheme. One notes from Table III that band gaps from our work are systematically larger than those obtained using the full-potential projector augmented wave (PAW) method;[33,34] this is mainly due to the use of pseudopotentials in this work. Nevertheless, the difference between our results and PAW results are mostly shifts within 0.1 eV (not shown), similar to that found in Ref. 39. On the other hand, we notice a larger difference in Γ_{1v}, X_{1c}, and E_g computed from our pseudopotential method and from the full-potential linear muffin-tin orbital method,[32] both at the G_0W_0 level and the QPscGW level. Such discrepancy is probably caused not only by the use of pseudopotentials in our work but also by the use of different basis sets in the two calculations, e.g., plane waves and mixed basis.

*ynli@ucdavis.edu

[1] M. D. Kelzenberg, S. W. Boettcher, J. A. Petykiewicz, D. B. Turner-Evans, M. C. Putnam, E. L. Warren, J. M. Spurgeon, R. M. Briggs, N. S. Lewis, and H. A. Atwater, Nature Mater. **9**, 239 (2010).

[2] S. W. Boettcher, J. M. Spurgeon, M. C. Putnam, E. L. Warren, D. B. Turner-Evans, M. D. Kelzenberg, J. R. Maiolo, H. A. Atwater, and N. S. Lewis, Science **327**, 185 (2010).

[3] A. Bansal, X. Li, S. I. Yi, W. H. Weinberg, and N. S. Lewis, J. Phys. Chem. B **105**, 10266 (2001).

[4] L. J. Webb and N. S. Lewis, J. Phys. Chem. B **107**, 5404 (2003).

[5] L. E. O'Leary, E. Johansson, B. S. Brunschwig, and N. S. Lewis, J. Phys. Chem. B (to be published).

[6] S. D. Solares, D. J. Michalak, W. A. Goddard, and N. S. Lewis, J. Phys. Chem. B **110**, 8171 (2006).

[7] E. J. Nemanick, S. D. Solares, W. A. Goddard, and N. S. Lewis, J. Phys. Chem. B **110**, 14842 (2006).
[8] Y. Kanai and A. Selloni, J. Am. Chem. Soc. **128**, 3892 (2006).
[9] K. C. Pandey, Phys. Rev. B **14**, 1557 (1976).
[10] X. Blase, X. Zhu, and S. G. Louie, Phys. Rev. B **49**, 4973 (1994).
[11] T. Yamada, M. Kawai, A. Wawro, S. Suto, and A. Kasuya, J. Chem. Phys. **121**, 10660 (2004).
[12] H. Yu, L. J. Webb, J. R. Heath, and N. S. Lewis, Appl. Phys. Lett. **88**, 252111 (2006).
[13] P. Giannozzi, S. Baroni, N. Bonini, M. Calandra, R. Car, C. Cavazzoni, D. Ceresoli, G. L. Chiarotti, M. Cococcioni, I. Dabo, A. Dal Corso, S. de Gironcoli, S. Fabris, G. Fratesi, R. Gebauer, U. Gerstmann, C. Gougoussis, A. Kokalj, M. Lazzeri, L. Martin-Samos, N. Marzari, F. Mauri, R. Mazzarello, S. Paolini, A. Pasquarello, L. Paulatto, C. Sbraccia, S. Scandolo, G. Sclauzero, A. P. Seitsonen, A. Smogunov, P. Umari, and R. M. Wentzcovitch, J. Phys.: Condens. Matter **21**, 395502 (2009).
[14] H. J. Monkhorst and J. D. Pack, Phys. Rev. B **13**, 5188 (1976).
[15] A. Aliano, Y. Li, G. Cicero, and G. Galli, J. Phys. Chem. C **114**, 11898 (2010).
[16] X. Gonze, B. Amadon, P.-M. Anglade, J.-M. Beuken, F. Bottin, P. Boulanger, F. Bruneval, D. Caliste, R. Caracas, M. Cote, T. Deutsch, L. Genovese, Ph. Ghosez, M. Giantomassi, S. Goedecker, D. R. Hamann, P. Hermet, F. Jollet, G. Jomard, S. Leroux, M. Mancini, S. Mazevet, M. J. T. Oliveira, G. Onida, Y. Pouillon, T. Rangel, G.-M. Rignanese, D. Sangalli, R. Shaltaf, M. Torrent, M. J. Verstraete, G. Zerah, and J. W. Zwanziger, Comput. Phys. Commun. **180**, 2582 (2009).
[17] X. Gonze, G.-M. Rignanese, M. Verstraete, J.-M. Beuken, Y. Pouillon, R. Caracas, F. Jollet, M. Torrent, G. Zerah, M. Mikami, P. Ghosez, M. Veithen, J.-Y. Raty, V. Olevano, F. Bruneval, L. Reining, R. Godby, G. Onida, D. Hamann, and D. Allan, Z. Kristallogr. **220**, 558 (2005).
[18] S. Lebègue, B. Arnaud, M. Alouani, and P. E. Bloechl, Phys. Rev. B **67**, 155208 (2003).
[19] R. W. Godby and R. J. Needs, Phys. Rev. Lett. **62**, 1169 (1989).
[20] M. S. Hybertsen and S. G. Louie, Phys. Rev. B **34**, 5390 (1986).
[21] B. Delley and E. F. Steigmeier, Appl. Phys. Lett. **67**, 2370 (1995).
[22] F. Bruneval, N. Vast, and L. Reining, Phys. Rev. B **74**, 045102 (2006).
[23] K. Hricovini, R. Günther, P. Thiry, A. Taleb-Ibrahimi, G. Indlekofer, J. E. Bonnet, P. Dumas, Y. Petroff, X. Blase, X. Zhu, S. G. Louie, Y. J. Chabal, and P. A. Thiry, Phys. Rev. Lett. **70**, 1992 (1993).
[24] *Semiconductors. Physics of Group IV Elements and III-V Compounds*, edited by K.-H. Hellwege and O. Madelung, Landolt-Bórnstein, New Series, Group III, Vol. 17, Pt. A (Springer, Berlin, 1982).
[25] H. Yu, L. J. Webb, R. S. Ries, S. D. Solares, W. A. Goddard, J. R. Heath, and N. S. Lewis, J. Phys. Chem. B **109**, 671 (2005).
[26] R. Hunger, R. Fritsche, B. Jaeckel, W. Jaegermann, L. J. Webb, and N. S. Lewis, Phys. Rev. B **72**, 045317 (2005).
[27] G. Heimel, L. Romaner, J.-L. Brédas, and E. Zojer, Surf. Sci. **600**, 4548 (2006).
[28] S. Watanabe, M. Aono, and M. Tsukada, J. Vac. Sci. Technol. B **12**, 2167 (1994).
[29] P. Sautet, J. Dunphy, D. Ogletree, and M. Salmeron, Surf. Sci. **295**, 347 (1993).
[30] H. Ness and A. J. Fisher, Phys. Rev. B **55**, 10081 (1997).
[31] H. Ness and A. J. Fisher, Phys. Rev. B **56**, 12469 (1997).
[32] T. Kotani, M. van Schilfgaarde, and S. V. Faleev, Phys. Rev. B **76**, 165106 (2007).
[33] M. Shishkin, M. Marsman, and G. Kresse, Phys. Rev. Lett. **99**, 246403 (2007).
[34] M. Shishkin and G. Kresse, Phys. Rev. B **75**, 235102 (2007).
[35] J. E. Ortega and F. J. Himpsel, Phys. Rev. B **47**, 2130 (1993).
[36] R. Shaltaf, G.-M. Rignanese, X. Gonze, F. Giustino, and A. Pasquarello, Phys. Rev. Lett. **100**, 186401 (2008).
[37] Y. Li, D. Lu, and G. Galli, J. Chem. Theory Comput. **5**, 881 (2009).
[38] E. L. Shirley, Phys. Rev. B **54**, 7758 (1996).
[39] M. Shishkin and G. Kresse, Phys. Rev. B **74**, 035101 (2006).